Received October 17, 2017, accepted November 10, 2017, date of publication November 20, 2017,
date of current version December 22, 2017.

Digital Object Identifier 10.1109/ACCESS.2017.2775250

Controller Design for a Variable-Speed Direct-Drive Permanent Magnet Synchronous Generator-Based Grid-Interfaced Wind Energy Conversion System Using D-Partition Technique

SAURABH MANI TRIPATHI[1], AMAR NATH TIWARI[2], AND DEEPENDRA SINGH[1]
[1]Department of Electrical Engineering, Kamla Nehru Institute of Technology, Sultanpur 228118, India
[2]Department of Electrical Engineering, M. M. M. University of Technology, Gorakhpur 273010, India

Corresponding author: Saurabh Mani Tripathi (mani_excel@yahoo.co.in)

This work was supported by the World Bank Assisted Technical Education Quality Improvement Programme (TEQIP-III), Kamla Nehru Institute of Technology, Sultanpur, India.

ABSTRACT In order to overcome the often encountered trouble in setting the controller parameters by trial and error, an attempt has been made to design the proportional-plus-integral (PI) controllers for a variable-speed direct-drive permanent magnet synchronous generator-based grid-connected wind energy system (WES). The characteristic equations for various control loops in WES have been developed, and the most stable zones have been identified in the parametric plane by means of the D-partition technique and frequency scanning check. To ensure high degree of relative system stability and good damping ratio, the PI controller parameters have been selected by comparing the step responses of the control loop plotted for different sets of controller parameters chosen from the identified stable zone. A simulation model using MATLAB/Simulink and SimPowerSystems toolbox has been built to examine the performance of the WES incorporated with the designed values of the parameters of the PI controllers under fluctuating wind speed condition.

INDEX TERMS Characteristic equation, D-partition technique, proportional-plus-integral (PI) controller design, relative system stability, wind energy system (WES).

I. INTRODUCTION

The amount of power generated by a wind energy system (WES) depends not only on the wind speed at the site, but also depends on the control system design adopted for the WES to cope with the intermittency and unpredictable nature of the wind. In recent years, the variable-speed direct-drive PMSGs offering less maintenance, higher efficiency, better power factor and gearless operation are becoming the most promising solution for the modern grid-interfaced WESs [1]–[4]. In many studies, the researchers have investigated a number of control strategies for the PMSG-based WES so as to develop such a system which being simple, reliable, robust, and capable of handling those disturbances which do affect its operation [2]. Nevertheless, the control system design for the PMSG-based WES with full-rating power converter configuration still needs to be improved so as to make the WES more suitable to be interfaced to the power grid. The design and optimization of the controller parameters is one of the most important tasks to be carried out during the commissioning of the control system. Thus, there are always the needs for simple and intuitive controller design techniques offering the optimal and robust control performances [4], [5]. The controllers based on proportional-plus-integral (PI) control-law offer the straightforward and the most efficient solution to the control system problems [6], [7]. For the design of the PI controllers in the control structure of a system, three fundamental objectives i.e. less overshoot, better damping and the least settling time need to be achieved [4], [8]. A number of techniques to design the parameters of the PI controller are summarized in [4], [5], [9], and [10]. In fact, each of the PI controller design technique has its own advantages and limitations [4]. The D-partitioning (or D-decomposition or domain separation) is an extremely powerful frequency-response technique to

study the effect on system's relative stability and transient performance when considering two parameters simultaneously (on which the coefficients of the characteristic equation depend) [11]–[14]. This technique was first developed by Neimark [15] and was generalized by Siljak [16]–[18]. It offers a possibility of defining the system's relative stability with the roots of the characteristic equation which lie within a specified p-plane of two adjustable parameters as coordinate axis termed as 'parametric-plane' [11], [12], [14]. This technique is particularly valuable for designing the parameters of PI controller for higher-order systems so as to achieve a given performance requirement by deriving the boundary curves for the system stability with specified damping in the parametric-plane [11], [14], [19], [20]. Some other advantages of the D-partition technique [21] are–(i) it is possible to study the effect of the transportation lag using this technique, (ii) algebraic manipulations do not increase considerably with the order of the control system, and (iii) control over transient response is possible by an appropriate choice of the adjustable parameters. The applicability of the D-partition technique has been documented in several research studies. A few of these researches are quoted in the following paragraphs.

Spal [22] generalized the method of the D-decomposition to the parametric-spaces of more than two dimensions and of more general regions of root plane than that of stability. Nanda [11] used the D-partition technique to determine the stabilizing gains in fast acting electronic excitation voltage controller so as to achieve maximum steady-state stability of a two-machine system. The D-partition technique has been applied in the work reported in [13] also in order to optimize the derivative-gain settings of the excitation voltage regulators of a power station for the maximum alternator stability and the best transient response. Pai and Ganesan [21] presented a systematic procedure using the D-partition technique to examine the effect of the parameter variations on the regions of the absolute and relative stability of a load frequency control system. The relative stability curves have been obtained for different governor systems in order to achieve optimum governor settings for a desired transient response [21]. Pandey and Tripathi [12] and Agrawal and Verma [23] derived the linearized characteristic equations by perturbing the system operating-variables about steady-state operating-points in order to determine the parameters of the current and speed PI controllers for a current-source-inverter (CSI)-fed induction motor (IM) drive using D-partition technique. Furthermore, a design approach based on the D-partition technique in z–domain has been proposed in [24] to select the parameters of PI controllers for a microcomputer controlled CSI-fed IM drive. Nevertheless, the final selections of the PI controller parameters in [12], [23], and [24] are based on the comparison of the step responses of each control-loop individually for different points selected from respective zones of stability in the parametric planes. Ruszewski and Nartowicz [25] addressed the stability problem of a control system composed of a fractional-order controller and an inertial plant with time-delay. A simple computational method based on the D-partition technique has been presented in [25] to determine the boundaries of stability-regions in controller parameter-plane for the tuning of the fractional-order controller which satisfies the requirements of specified gain-and phase-margins. Yanev and Masupe [26] contributed in the design of a robust controller with two degrees-of-freedom for linear control systems using the D-partition technique so as to achieve a desired system damping, stability and time-response. Dubonjic *et al.* [27] proposed a procedure for the design of PI controller parameters for higher-order control systems based on the D-decomposition technique and demonstrated the superiority of this technique over some other techniques of PI controller design. Also, based on the D-partition technique and the cross-boundary theorem, a method for the estimation of the parameters of PID controllers has been introduced in [28] in order to satisfy a robust performance-constraint in the stability-region.

The work reported in this paper presents a systematic procedure for the design of the parameters of PI controllers involved in a grid-interfaced direct-drive PMSG-based WES using the D-partition technique in order to achieve the maximum system stability and the best closed-loop control performance. The problem has been formulated as follows–''Tune the parameters of the PI controllers in the control structures of a grid-interfaced PMSG-based wind energy system such that the maximum system stability and the best closed-loop control performance could be achieved''.

II. SYSTEM CONFIGURATION AND CONTROL

The configuration of the proposed WES comprises a surface-mount PMSG directly driven by variable-speed gearless wind turbine. The PMSG and power grid have been interfaced through a full-rating two-level back-to-back converters as shown in Fig.1. The calculations for the sizing/selection of various components of the proposed WES have already been reported by the authors in [4]. The PMSG rotor speed control has been performed by means of field-oriented control (FOC) of stator-side converter (SSC) wherein the reference rotor speed (ω_r^*), the reference electromagnetic torque (T_e^*), the reference d- and q- axes stator current components (i_{ds}^* and i_{qs}^*), and the reference three-phase stator currents (I_{sa}^*, I_{sb}^* and I_{sc}^*) have been calculated using (1)–(5) [4], [29], [30]. The hysteresis current controller (HCC) compares the actual three-phase stator currents with their reference values and generates the gating pulses for the SSC.

$$\omega_r^* = \lambda_{opt} V_w / R \tag{1}$$

$$T_e^* = K_{ps}\left(\frac{1+pT_{is}}{pT_{is}}\right)\cdot(\omega_r^* - \omega_r) \tag{2}$$

$$i_{ds}^* = 0 \tag{3}$$

$$i_{qs}^* = \left(\frac{4}{3\lambda_m P}\right)\cdot T_e^* \tag{4}$$

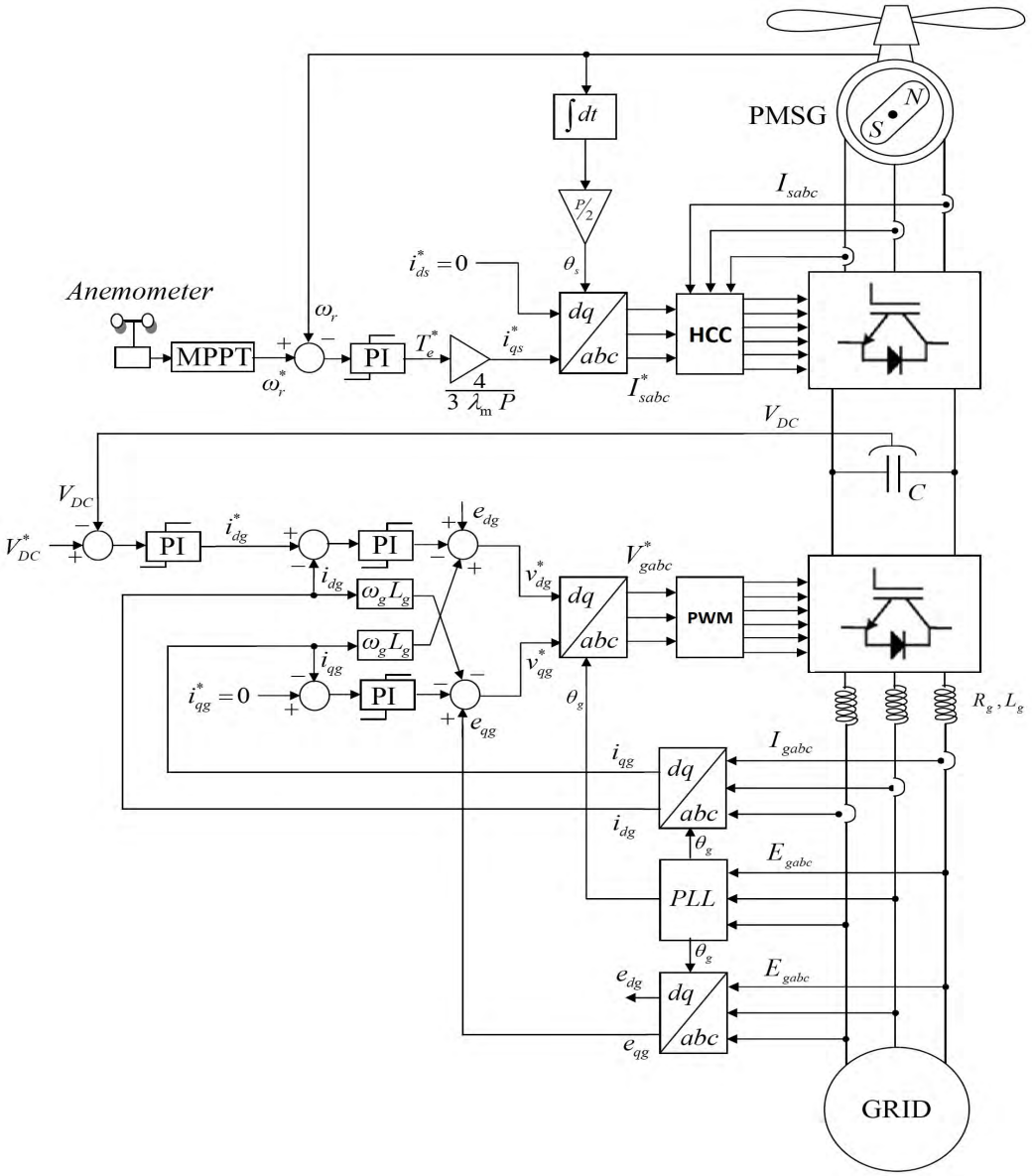

FIGURE 1. Proposed variable-speed direct-drive PMSG-based wind energy system (WES).

$$\begin{bmatrix} I^*_{sa} \\ I^*_{sb} \\ I^*_{sc} \end{bmatrix} = \begin{bmatrix} \sin(\omega_s t) & \sin\left(\omega_s t - \frac{2\pi}{3}\right) & \sin\left(\omega_s t + \frac{2\pi}{3}\right) \\ \cos(\omega_s t) & \cos\left(\omega_s t - \frac{2\pi}{3}\right) & \cos\left(\omega_s t + \frac{2\pi}{3}\right) \end{bmatrix}^{\mathrm{T}} \times \begin{bmatrix} i^*_{ds} \\ i^*_{qs} \end{bmatrix} \tag{5}$$

where, λ_{opt} is the optimal tip-speed-ratio of the turbine; V_w is the wind speed, R is the radius of the turbine-blades; K_{ps} and T_{is} are the proportional-gain and integral time-constant of the speed PI controller, respectively; ω_r and ω_s are the mechanical and electrical rotor speeds, respectively; λ_m is the permanent magnet flux and P is the number of generator poles.

In order to achieve the objectives of dc-link voltage control and unity-power-factor operation of the line-side converter (LSC), the voltage-oriented control (VOC) of LSC has been considered wherein, the reference d- and q- axes grid current components (i^*_{dg} and i^*_{qg}), the reference d- and q- axes LSC voltage components (v^*_{dg} and v^*_{qg}), and the reference three-phase LSC voltages (V^*_{ga}, V^*_{gb} and V^*_{gc}) have been calculated using (6)–(10) [4], [29], [30]. The grid angular frequency (ω_g), which is necessary for the grid-synchronization of the WES, has been determined by means of a phase-locked-loop (PLL) [31]. The reference three-phase LSC

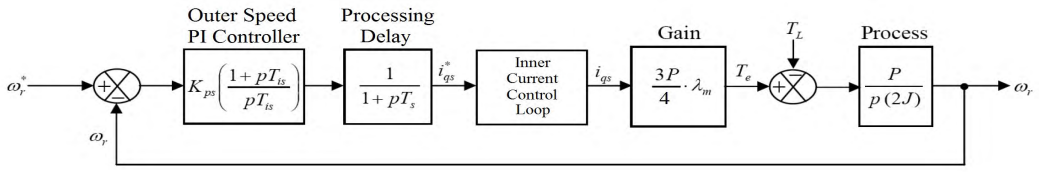

FIGURE 2. Mathematical block-diagram of the rotor speed control loop.

voltages V_{gabc}^* have been applied to the PWM controller to generate the gating pulses for the LSC.

$$i_{dg}^* = K_{pv}\left(\frac{1+pT_{iv}}{pT_{iv}}\right)\cdot(V_{DC}^* - V_{DC}) \tag{6}$$

$$i_{qg}^* = 0 \tag{7}$$

$$v_{dg}^* = e_{dg} + \omega_g L_g i_{qg} - K_{pc}\left(\frac{1+pT_{ic}}{pT_{ic}}\right)\cdot(i_{dg}^* - i_{dg}) \tag{8}$$

$$v_{qg}^* = e_{qg} - \omega_g L_g i_{dg} - K_{pc}\left(\frac{1+pT_{ic}}{pT_{ic}}\right)\cdot(i_{qg}^* - i_{qg}) \tag{9}$$

$$\begin{bmatrix} V_{ga}^* \\ V_{gb}^* \\ V_{gc}^* \end{bmatrix} = \begin{bmatrix} \sin(\omega_g t) & \sin\left(\omega_g t - \frac{2\pi}{3}\right) & \sin\left(\omega_g t + \frac{2\pi}{3}\right) \\ \cos(\omega_g t) & \cos\left(\omega_g t - \frac{2\pi}{3}\right) & \cos\left(\omega_g t + \frac{2\pi}{3}\right) \end{bmatrix}^{\mathrm{T}} \times \begin{bmatrix} v_{dg}^* \\ v_{qg}^* \end{bmatrix} \tag{10}$$

where, K_{pv} and T_{iv} are the proportional-gain and integral time-constant of the dc-link voltage PI controller, respectively; V_{DC}^* and V_{DC} are the reference and actual values of dc-link voltages, respectively; e_{dg} and e_{qg} are the d- and q-axes grid voltage components, respectively; i_{dg} and i_{qg} are the actual d- and q- axes grid current components, respectively; K_{pc} and T_{ic} are the proportional-gain and the integral time-constant of the grid current PI controllers, respectively.

III. DESIGN OF THE PI CONTROLLER PARAMETERS USING THE D-PARTITION TECHNIQUE

The satisfactory performance of the WES depends on the design of the parameters of the PI controllers in different control-loops. The parameters of the PI controllers employed in various control-loops can be designed on the basis of the system's relative stability and transient performance using the D-partition technique.

A. DESIGN OF THE SPEED PI CONTROLLER

Considering the transfer function of the HCC-based current control block as 'unitary-gain' [4], the open-loop transfer function of the rotor speed control loop as depicted in Fig. 2 can be modeled as follows

$$G_{OMS}(p) = K_{ps}\left(\frac{1+pT_{is}}{pT_{is}}\right)\cdot\left(\frac{1}{1+pT_s}\right)\cdot\left(\frac{3}{4}\lambda_m P\right)\cdot\frac{P}{p(2J)} \tag{11}$$

where, T_s is the sample-time for the speed control loop and J is the turbine-generator inertia.

The closed-loop transfer function of the rotor speed control loop can be expressed as follows

$$G_{CMS}(p) = \frac{G_{OMS}(p)}{1+G_{OMS}(p)} \tag{12}$$

The response of the rotor speed control-loop owing to the alteration in the disturbance-signal input can be obtained from the transfer function expressed as follows

$$G_{DMS}(p) = -\frac{G_{PMS}(p)}{1+G_{OMS}(p)} \tag{13}$$

where

$$G_{PMS}(p) = \frac{P}{p(2J)} \tag{14}$$

Then, the characteristic equation of the rotor speed control loop can be given as follows

$$D_{MS}(p) = 1 + G_{OMS}(p) = 0 \tag{15}$$

To plot the D-partition boundary in the K_{ps}-K_{is} plane, (15) can be expressed as follows

$$K_{ps}F_4(p) + K_{is}F_5(p) + F_6(p) = 0 \tag{16}$$

where

$$F_6(p) = p^3F_2(p) + p^2F_3(p) \tag{17}$$

$$F_5(p) = F_1(p) \tag{18}$$

$$F_4(p) = pF_1(p) \tag{19}$$

$$F_3(p) = 8J \tag{20}$$

$$F_2(p) = 8JT_s \tag{21}$$

$$F_1(p) = 3\lambda_m P^2 \tag{22}$$

Since p is the complex frequency, the real-and imaginary-parts of (16) can be separated as follows

$$K_{ps}\cdot\Re_e[F_4(p)] + K_{is}\cdot\Re_e[F_5(p)] + \Re_e[F_6(p)] = 0 \tag{23}$$

$$K_{ps}\cdot\Im_m[F_4(p)] + K_{is}\cdot\Im_m[F_5(p)] + \Im_m[F_6(p)] = 0 \tag{24}$$

Solving (23)-(24), the values for K_{ps} and K_{is} can be given as follows

$$K_{ps} = \frac{\begin{vmatrix} -\Re_e[F_6(p)] & \Re_e[F_5(p)] \\ -\Im_m[F_6(p)] & \Im_m[F_5(p)] \end{vmatrix}}{\Delta_{ms}} \tag{25}$$

$$K_{is} = \frac{\begin{vmatrix} \Re_e[F_4(p)] & -\Re_e[F_6(p)] \\ \Im_m[F_4(p)] & -\Im_m[F_6(p)] \end{vmatrix}}{\Delta_{ms}} \tag{26}$$

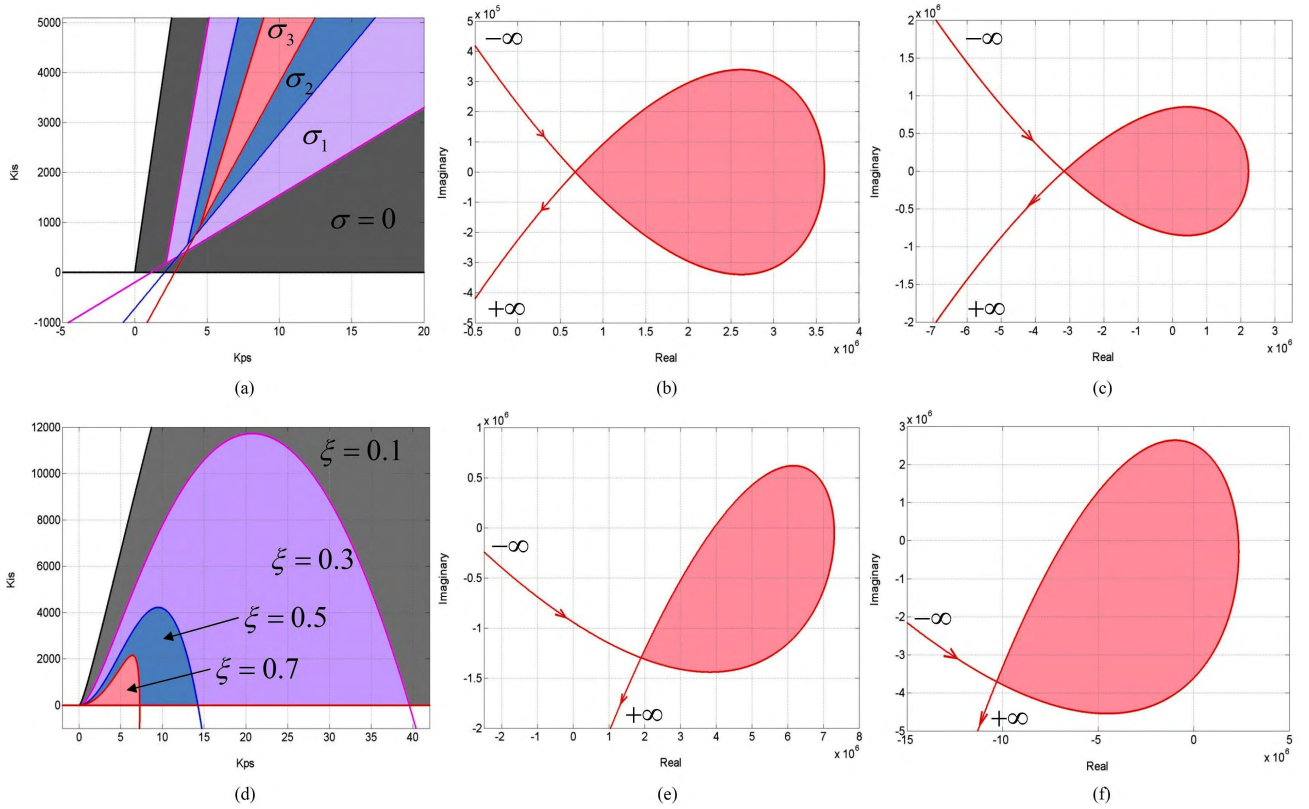

FIGURE 3. (a). D-partition boundaries for the speed PI controller design with different values of $\sigma(\sigma_3 > \sigma_2 > \sigma_1 > 0)$. (b). Frequency scanning for the point ($\sigma = 0.0, K_{ps} = 1.3, K_{is} = 3200$) located outside the shaded zone of (a)—-UNSTABLE. (c). Frequency scanning for the point ($\sigma = 0.0, K_{ps} = 2.4, K_{is} = 1980$) located inside the shaded zone of (a)—-STABLE. (d). D-partition boundaries for the speed PI controller design with different values of ξ. (e). Frequency scanning for the point ($\xi = 0.1, K_{ps} = 2.5, K_{is} = 6500$) located outside the shaded zone of (d)—-UNSTABLE. (f). Frequency scanning for the point ($\xi = 0.1, K_{ps} = 6.0, K_{is} = 2085$) located inside the shaded zone of (d)—-STABLE.

where

$$\Delta_{ms} = \begin{vmatrix} \Re_e[F_4(p)] & \Re_e[F_5(p)] \\ \Im_m[F_4(p)] & \Im_m[F_5(p)] \end{vmatrix} \tag{27}$$

Substituting $p = (-\sigma + j\omega)$ in (25)–(27) and varying ω from $-\infty$ to $+\infty$ for fixed σ, it is possible to find sets of values of K_{ps} and K_{is} with high-degree of relative system stability [11]–[13], [23], [24], [32]. Such sets of values can be plotted as a gain-locus in the K_{ps}-K_{is} plane called the D-partition boundary as shown in Fig. 3(a) which divides the parametric-plane in the stable and unstable domains. While moving along the boundary of the D-partition in the direction of ω increasing, the boundary has been shaded on the left-edge at those points for which $\Delta_{ms} > 0$ and on the right-edge at those points for which $\Delta_{ms} < 0$ [14], [23]. The zone in the sense of shading in the parametric-plane is the probable zone of stability. The stability of the shaded zone can further be confirmed by the frequency scanning technique wherein the characteristic vector $D_{MS}(p) = K_{ps}F_4(p) + K_{is}F_5(p) + F_6(p)$ has been plotted in the real-imaginary plane firstly selecting a point ($\sigma = 0.0, K_{ps} = 1.3, K_{is} = 3200$) located outside the shaded zone. The locus of $D_{MS}(p)$ has been shaded to the left with the variation in ω from $-\infty$ to $+\infty$.

As shown in Fig.3 (b), the origin is not enclosed by the locus of the characteristic vector and hence, the zone outside the shaded one is unstable in the parametric-plane. Again, the characteristic vector $D_{MS}(p)$ has been plotted in the real-imaginary plane selecting another point ($\sigma = 0.0, K_{ps} = 2.4, K_{is} = 1980$) located inside the shaded zone and the locus of $D_{MS}(p)$ has been shaded on the left-edge with the variation in ω from $-\infty$ to $+\infty$. As shown in Fig. 3 (c), the origin is enclosed by the locus of the characteristic vector and hence, the shaded zone is stable in the parametric-plane and any point within it can be considered as a stable point.

For absolute stability σ is taken zero. However, to ensure maximum relative system stability, σ has gradually been increased and the D-partition boundaries have been plotted as depicted in Fig. 3 (a). It can be observed that the zone of stability shrinks while σ increasing and after a certain value of σ, the most stable zone can be identified [12], [23], [24]. Here, the innermost zone shaded with the red color in Fig. 3(a) is the most stable zone with high-degree of relative system stability.

The D-partition boundary can also be plotted by substituting $p = \left(-\xi\omega_n + j\omega_n\sqrt{1-\xi^2}\right)$ (where, ω_n is the undamped natural frequency) in (25)–(27) for the fixed value of damping ratio $\xi(> 0)$ and probable zone of stability in the sense of shading has been obtained as shown in Fig. 3(d). The stability of the shaded zone can further be confirmed by the frequency-scanning technique for the points outside and

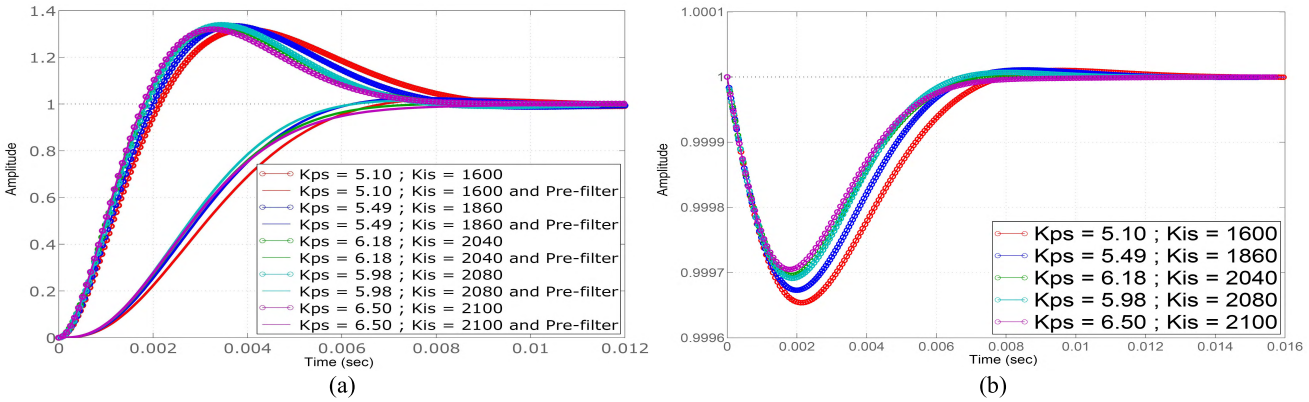

FIGURE 4. (a) Step responses and (b) disturbance rejection capability of the PMSG rotor speed control loop for different sets of K_{ps} and K_{is} values chosen from the common portion of the most stable zones in Fig.3.

TABLE 1. Performance of the rotor speed control loop corresponding to different sets of K_{ps} and K_{is} values.

K_{ps}	K_{is}	T_{is}	Step Response				Disturbance Rejection Capability	
			Without Pre-filter		With Pre-filter			
			Overshoot (%)	Settling Time (ms)	Overshoot (%)	Settling Time (ms)	Undershoot (%)	Settling Time (ms)
5.10	1600	0.0032	31.9	8.65	2.39	9.55	0.035	11.10
5.49	1860	0.0030	33.4	7.85	2.55	8.79	0.033	10.20
6.18	2040	0.0030	32.6	7.45	---	6.45	0.030	6.95
5.98	2080	0.0029	33.9	7.31	1.41	5.75	0.031	8.67
6.50	2100	0.0031	32.0	7.36	---	7.21	0.030	7.48

inside the shaded zone. For frequency-scanning, the loci of the characteristic vector for the points ($\xi = 0.1, K_{ps} = 2.5, K_{is} = 6500$) and ($\xi = 0.1, K_{ps} = 6.0, K_{is} = 2085$) located outside and inside the shaded zone, respectively are shown in Fig. 3 (e)-(f) and it can be confirmed that the shaded zone is stable in the parametric-plane.

To ensure high damping ratio, ξ has gradually been increased and the D-partition boundaries have been plotted as depicted in Fig. 3 (d). Again it can be seen that the zone of stability shrinks while ξ increasing and after a sufficient value of ξ, the most stable zone can be identified. Here, the innermost zone shaded with the red color in Fig. 3 (d) is the most stable zone with specified damping ratio. The final selection of the parameters of speed PI controller has been made by comparing the step response curves as well as investigating the disturbance rejection capability of the speed control loop as shown in Fig. 4 for different sets of K_{ps} and K_{is} values chosen from the common portion of the most stable zones in Fig.3 identified earlier to ensure the desired relative system stability and damping ratio, respectively.

Large peak overshoots in the step responses of the rotor speed control loop can be observed. So, a first order pre-filter $G_{FMS}(p)$ can also be employed on the reference signal which decreases the peak overshoot [8] and enhances the performance of the speed PI controller.

$$G_{FMS}(p) = \frac{K_{is}}{K_{is} + pK_{ps}} \tag{28}$$

Thus, the closed-loop transfer function $G_{CMS}(p)$ reduces to

$$G_{CFMS}(p) = G_{FMS}(p) \cdot G_{CMS}(p) \tag{29}$$

The performance of the rotor speed control-loop corresponding to different sets of K_{ps} and K_{is} values have been summarized in Table–1. On comparison, it has been found that the step response (with pre-filter on the reference signal) corresponding to ($K_{ps} = 5.98$ and $K_{is} = 2080$) is fast enough with acceptable percentage peak overshoot. Further, the disturbance rejection capability of the rotor speed control-loop is also the moderate one corresponding to ($K_{ps} = 5.98$ and $K_{is} = 2080$). Hence, the selected transfer function of the speed PI controller is given by

$$G_{cs}(p) = 5.98\left(\frac{1 + 0.0029p}{0.0029p}\right) \tag{30}$$

B. DESIGN OF THE GRID CURRENT PI CONTROLLERS

The open-loop transfer function of the grid current control loops as depicted in Fig. 5 can be modeled as follows

$$G_{OGC}(p) = K_{pc}\left(\frac{1 + pT_{ic}}{pT_{ic}}\right) \cdot \left(\frac{1}{1 + pT_c}\right) \cdot \left(\frac{1}{1 + 0.5pT_c}\right) \cdot \left(\frac{K_{gc}}{1 + pT_{gc}}\right) \tag{31}$$

where, $K_{gc} = 1/R_g$, $T_{gc} = L_g/R_g$ and, T_c is the sample-time for the grid current control loop.

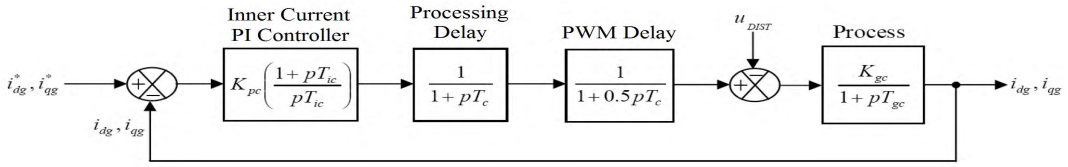

FIGURE 5. Mathematical block-diagram of the grid current control loop.

The closed-loop transfer function of the grid current control loop can be expressed as follows

$$G_{CGC}(p) = \frac{G_{OGC}(p)}{1 + G_{OGC}(p)} \tag{32}$$

The response of the grid current control loop owing to the alteration in the disturbance signal input can be obtained from the transfer function expressed as follows

$$G_{DGC}(p) = -\frac{G_{PGC}(p)}{1 + G_{OGC}(p)} \tag{33}$$

where

$$G_{PGC}(p) = K_{gc}/(1 + pT_{gc}) \tag{34}$$

Then, the characteristic equation of the grid current control loop can be given as follows

$$D_{GC}(p) = 1 + G_{OGC}(p) = 0 \tag{35}$$

To plot the D-partition boundary in the K_{pc}-K_{ic} plane, (35) can be expressed as follows

$$K_{pc}F_{15}(p) + K_{ic}F_{16}(p) + F_{17}(p) = 0 \tag{36}$$

where

$$F_{17}(p) = p^4F_8(p) + p^3F_{13}(p) + p^2F_{14}(p) + 2p \tag{37}$$
$$F_{16}(p) = F_7(p) \tag{38}$$
$$F_{15}(p) = pF_7(p) \tag{39}$$
$$F_{14}(p) = F_{11}(p) + F_{12}(p) \tag{40}$$
$$F_{13}(p) = F_9(p) + F_{10}(p) \tag{41}$$
$$F_{12}(p) = 2T_{gc} \tag{42}$$
$$F_{11}(p) = 3T_c \tag{43}$$
$$F_{10}(p) = 3T_{gc}T_c \tag{44}$$
$$F_9(p) = T_c^2 \tag{45}$$
$$F_8(p) = T_c^2T_{gc} \tag{46}$$
$$F_7(p) = 2K_{gc} \tag{47}$$

The real and imaginary parts of (36) can be separated as follows

$$K_{pc} \cdot \Re_e[F_{15}(p)] + K_{ic} \cdot \Re_e[F_{16}(p)] + \Re_e[F_{17}(p)] = 0 \tag{48}$$

$$K_{pc} \cdot \Im_m[F_{15}(p)] + K_{ic} \cdot \Im_m[F_{16}(p)] + \Im_m[F_{17}(p)] = 0 \tag{49}$$

Solving (48)-(49), the values for K_{pc} and K_{ic} can be given as follows

$$K_{pc} = \frac{\begin{vmatrix} -\Re_e[F_{17}(p)] & \Re_e[F_{16}(p)] \\ -\Im_m[F_{17}(p)] & \Im_m[F_{16}(p)] \end{vmatrix}}{\Delta_{gc}} \tag{50}$$

$$K_{ic} = \frac{\begin{vmatrix} \Re_e[F_{15}(p)] & -\Re_e[F_{17}(p)] \\ \Im_m[F_{15}(p)] & -\Im_m[F_{17}(p)] \end{vmatrix}}{\Delta_{gc}} \tag{51}$$

where

$$\Delta_{gc} = \begin{vmatrix} \Re_e[F_{15}(p)] & \Re_e[F_{16}(p)] \\ \Im_m[F_{15}(p)] & \Im_m[F_{16}(p)] \end{vmatrix} \tag{52}$$

Substituting $p = (-\sigma + j\omega)$ in (50)–(52) and varying ω from $-\infty$ to $+\infty$ for fixed σ, D-partition boundary has been plotted and shaded on the left-edge at those points for which $\Delta_{gc} > 0$ and on the right-edge at those points for which $\Delta_{gc} < 0$ while moving along the boundary of the D-partition in the direction of ω increasing in order to identify the stable and unstable domains in the parametric-plane [14], [23] as shown in Fig. 6(a). The zone in the sense of shading in the parametric-plane is the probable zone of stability. For further confirmation of the stability of shaded zone by means of the frequency scanning technique, the loci of the characteristic vector $D_{GC}(p) = K_{pc}F_{15}(p) + K_{ic}F_{16}(p) + F_{17}(p)$ for the points ($\sigma = 0.0, K_{pc} = 110, K_{ic} = 2000000$) and ($\sigma = 0.0, K_{pc} = 140, K_{ic} = 600000$) located outside and inside the shaded zone, respectively are shown in Fig. 6 (b)–(c). As shown in Fig. 6 (b), the origin is not enclosed by the locus of the characteristic vector and hence, the zone outside the shaded one is unstable in the parametric-plane. On the other hand, as shown in Fig. 6 (c) the origin is enclosed by the locus of the characteristic vector and hence, the shaded zone is stable in the parametric-plane and any point within it can be considered as a stable point.

For absolute stability σ is taken zero. However, to ensure the maximum relative system stability, σ has gradually been increased and the D-partition boundaries have been plotted as depicted in Fig. 6 (a). It can be observed that the zone of stability shrinks while σ increasing and after a certain value of σ, the most stable zone can be identified [12], [23], [24]. Here, the innermost zone shaded with the red color in Fig. 6 (a) is the most stable zone with high degree of relative system stability. The D-partition boundary has also been plotted by substituting $p = \left(-\xi\omega_n + j\omega_n\sqrt{1-\xi^2}\right)$ in (50)–(52) for the fixed value of damping ratio $\xi(> 0)$

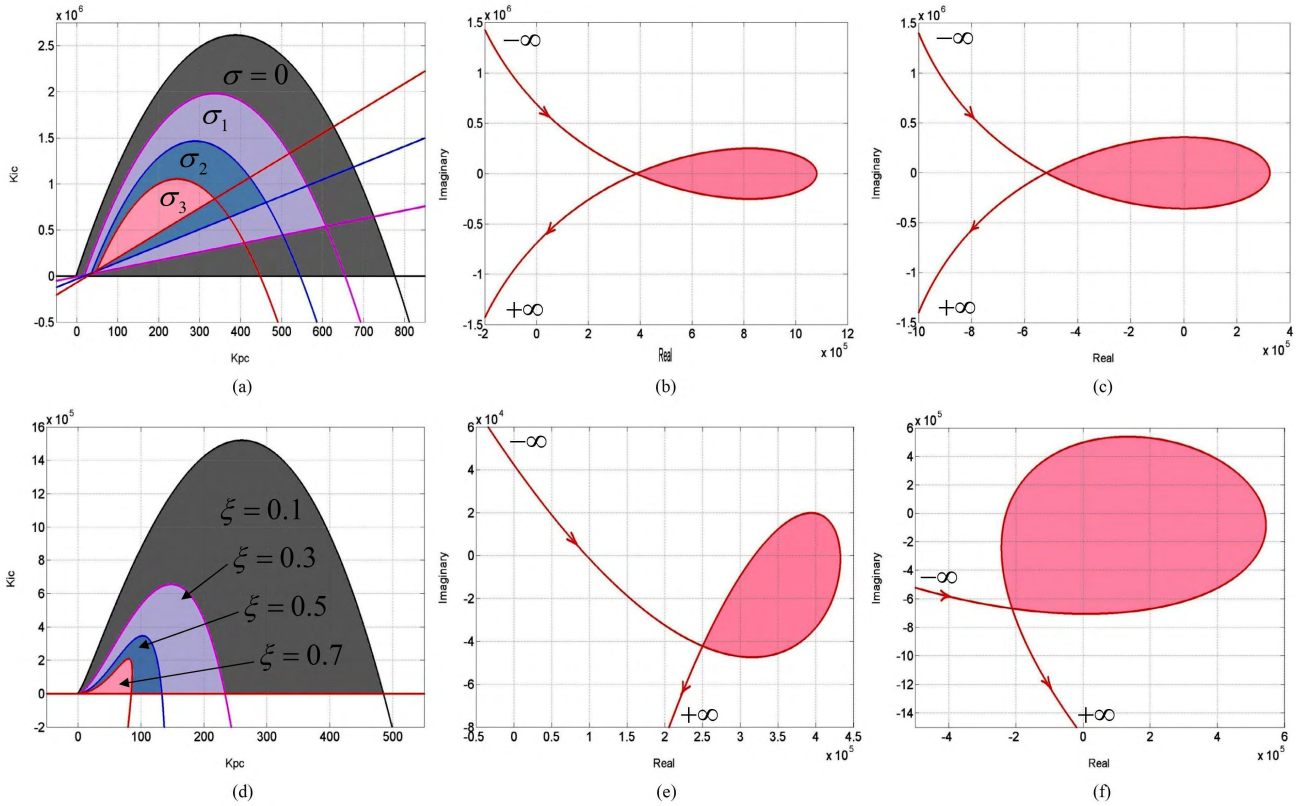

FIGURE 6. (a). D-partition boundaries for the grid current PI controller design with different values of $\sigma(\sigma_3 > \sigma_2 > \sigma_1 > 0)$. (b). Frequency scanning for the point ($\sigma = 0.0, K_{pc} = 110, K_{ic} = 2000000$) located outside the shaded zone of (a)—-UNSTABLE. (c). Frequency scanning for the point ($\sigma = 0.0, K_{pc} = 140, K_{ic} = 600000$) located inside the shaded zone of (a)—-STABLE. (d). D-partition boundaries for the grid current PI controller design with different values of ξ. (e). Frequency scanning for the point ($\xi = 0.1, K_{pc} = 25, K_{ic} = 800000$) located outside the shaded zone of (d)—-UNSTABLE. (f). Frequency scanning for the point ($\xi = 0.1, K_{pc} = 200, K_{ic} = 1000000$) located inside the shaded zone of (d)—-STABLE.

and probable zone of stability in the sense of shading has been obtained as shown in Fig. 6 (d). For frequency scanning in regards to further confirm the stability of the shaded zone, the loci of the characteristic vector $D_{GC}(p)$ for the points ($\xi = 0.1, K_{pc} = 25, K_{ic} = 800000$) and ($\xi = 0.1, K_{pc} = 200, K_{ic} = 1000000$) located outside and inside the shaded zone, respectively are shown in Fig. 6 (e)–(f) and it can be confirmed that the shaded zone is stable in the parametric-plane.

To ensure high damping ratio, ξ has gradually been increased and the D-partition boundaries have been plotted as depicted in Fig. 6 (d). Again it can be observed that the zone of stability shrinks while ξ increasing and after a sufficient value of ξ, the most stable zone can be identified. Here, the innermost zone shaded with the red color in Fig. 6 (d) is the most stable zone with specified damping ratio. The final selection of the current PI controller parameters has been made by comparing the step response curves as well as investigating the disturbance rejection capability of the grid current control loop as shown in Fig. 7 for different sets of K_{pc} and K_{ic} values chosen from the common portion of the most stable zones in Fig. 6 identified earlier to ensure the desired relative system stability and damping ratio, respectively. Large peak overshoots in the step responses of the grid current control loop can be observed. So, a first order pre-filter $G_{FGC}(p)$ can also be employed on the reference signal which decreases the peak overshoot [8] and enhances the performance of the grid current PI controllers.

$$G_{FGC}(p) = \frac{K_{ic}}{K_{ic} + pK_{pc}} \tag{53}$$

Thus, the closed-loop transfer function $G_{CGC}(p)$ reduces to

$$G_{CFGC}(p) = G_{FGC}(p) \cdot G_{CGC}(p) \tag{54}$$

The performance of the grid current control loop corresponding to different sets of K_{pc} and K_{ic} values have been summarized in Table–2. On comparison, it has been found that the step response curve (with pre-filter on the reference signal) corresponding to ($K_{pc} = 69$ and $K_{ic} = 160700$) settles very fast with acceptable percentage peak overshoot. Further, the disturbance rejection capability of the grid current control loop is also the moderate one corresponding to($K_{pc} = 69$ and $K_{ic} = 160700$). Hence, the selected transfer function of the grid current PI controller is given by

$$G_{cc}(p) = 69\left(\frac{1 + 0.00043p}{0.00043p}\right) \tag{55}$$

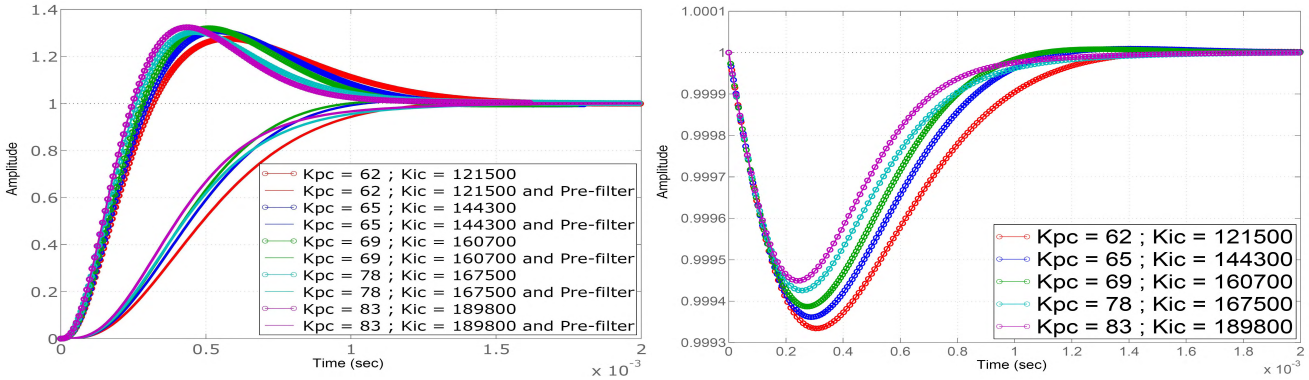

FIGURE 7. (a) Step responses and (b) disturbance rejection capability of the grid current control loop for different sets of K_{pc} and K_{ic} values chosen from the common portion of the most stable zones in Fig. 6.

TABLE 2. Performance of the grid current control loop corresponding to different sets of K_{pc} and K_{ic} values.

K_{pc}	K_{ic}	T_{ic}	Step Response				Disturbance Rejection Capability	
			Without Pre-filter		With Pre-filter			
			Overshoot (%)	Settling Time (ms)	Overshoot (%)	Settling Time (ms)	Undershoot (%)	Settling Time (ms)
62	1.215e5	0.00051	27.5	1.38	0.368	1.16	0.067	1.32
65	1.443e5	0.00045	30.6	1.22	1.260	0.95	0.064	1.09
69	1.607e5	0.00043	31.9	1.13	1.060	0.89	0.061	1.02
78	1.675e5	0.00047	30.3	1.15	---	1.21	0.057	1.30
83	1.898e5	0.00044	32.3	1.04	---	1.14	0.055	1.21

C. DESIGN OF DC-LINK VOLTAGE PI CONTROLLER

Approximating the grid current closed-loop transfer function (54), an equivalent transfer function of first-order can be obtained as follows

$$G_{GCL}(p) = \frac{1}{1 + pT_{GCL}} \tag{56}$$

where

$$T_{GCL} = (1 + K_{gc}K_{pc})/K_{gc}K_{ic} \tag{57}$$

Thus, the open-loop transfer function $G_{OGV}(p)$ of the dc-link voltage control-loop as depicted in Fig. 8 can be modeled as follows

$$G_{OGV}(p) = K_{pv}\left(\frac{1 + pT_{iv}}{pT_{iv}}\right)\left(\frac{1}{1 + pT_v}\right)\left(\frac{1}{1 + pT_{GCL}}\right) \times \left(\frac{3e_{dg}}{2V_{DC}}\right)\left(\frac{1}{pC}\right) \tag{58}$$

where, T_v is the sample-time for the dc-link voltage control loop.

The closed-loop transfer function of the dc-link voltage control loop can be expressed as follows

$$G_{CGV}(p) = \frac{G_{OGV}(p)}{1 + G_{OGV}(p)} \tag{59}$$

The response of the dc-link voltage control loop owing to the alteration in the disturbance signal input can be obtained from the transfer function expressed as follows

$$G_{DGV}(p) = -\frac{G_{PGV}(p)}{1 + G_{OGV}(p)} \tag{60}$$

where

$$G_{PGV}(p) = 1/pC \tag{61}$$

Then, the characteristic equation of the dc-link voltage control loop can be given as follows

$$D_{GV}(p) = 1 + G_{OGV}(p) = 0 \tag{62}$$

To plot the D-partition boundary in the $K_{pv} - K_{iv}$ plane, (62) can be expressed as follows

$$K_{pv}F_{28}(p) + K_{iv}F_{29}(p) + F_{30}(p) = 0 \tag{63}$$

where

$$F_{30}(p) = p^4F_{23}(p) + p^3F_{26}(p) + p^2F_{27}(p) \tag{64}$$
$$F_{29}(p) = F_{18}(p) \tag{65}$$
$$F_{28}(p) = pF_{18}(p) \tag{66}$$
$$F_{27}(p) = F_{21}(p) \cdot F_{22}(p) \tag{67}$$
$$F_{26}(p) = F_{24}(p) + F_{25}(p) \tag{68}$$
$$F_{25}(p) = F_{20}(p) \cdot F_{21}(p) \tag{69}$$
$$F_{24}(p) = [1 + F_{19}(p)] \cdot F_{22}(p) \tag{70}$$
$$F_{23}(p) = [1 + F_{19}(p)] \cdot F_{20}(p) \tag{71}$$
$$F_{22}(p) = 2CV_{DC} \tag{72}$$
$$F_{21}(p) = K_{gc}K_{ic} \tag{73}$$
$$F_{20}(p) = 2CT_vV_{DC} \tag{74}$$
$$F_{19}(p) = K_{gc}K_{pc} \tag{75}$$
$$F_{18}(p) = 3K_{gc}K_{ic}e_{dg} \tag{76}$$

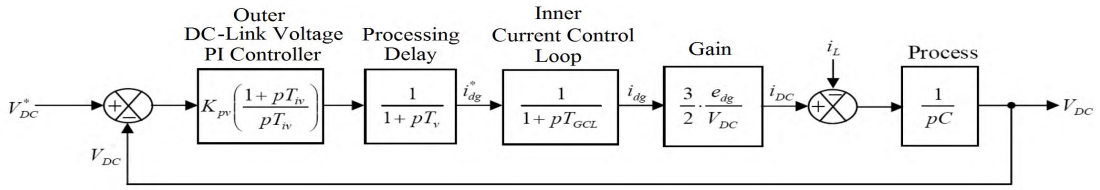

FIGURE 8. Mathematical block-diagram of the dc-link voltage control loop.

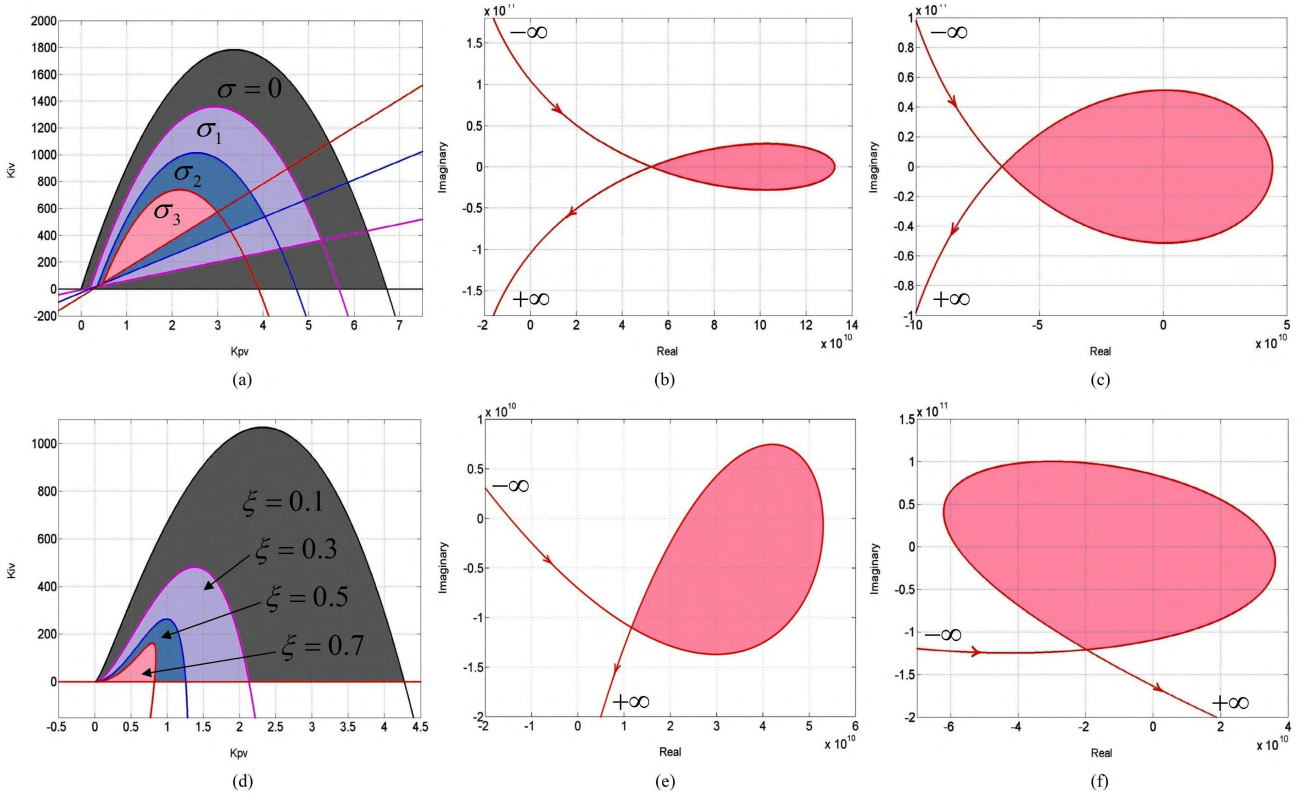

FIGURE 9. (a). D-partition boundaries for the dc-link voltage PI controller design with different values of $\sigma(\sigma_3 > \sigma_2 > \sigma_1 > 0)$. (b). Frequency scanning for the point ($\sigma = 0.0, K_{pv} = 1.0, K_{iv} = 1500$) located outside the shaded zone of (a)—-UNSTABLE. (c). Frequency scanning for the point ($\sigma = 0.0, K_{pv} = 1.5, K_{iv} = 500$) located inside the shaded zone of (a)—-STABLE. (d). D-partition boundaries for the dc-link voltage PI controller design with different values of ξ. (e). Frequency scanning for the point ($\xi = 0.1, K_{pv} = 0.5, K_{iv} = 600$) located outside the shaded zone of (d)—-UNSTABLE. (f). Frequency scanning for the point ($\xi = 0.1, K_{pv} = 2.5, K_{iv} = 400$) located inside the shaded zone of (d)—-STABLE.

The real and imaginary parts of (63) can be separated as follows

$$K_{pv} \cdot \Re_e[F_{28}(p)] + K_{iv} \cdot \Re_e[F_{29}(p)] + \Re_e[F_{30}(p)] = 0 \quad (77)$$

$$K_{pv} \cdot \Im_m[F_{28}(p)] + K_{iv} \cdot \Im_m[F_{29}(p)] + \Im_m[F_{30}(p)] = 0 \quad (78)$$

Solving (77)-(78), the values for K_{pv} and K_{iv} can be given as follows

$$K_{pv} = \frac{\begin{vmatrix} -\Re_e[F_{30}(p)] & \Re_e[F_{29}(p)] \\ -\Im_m[F_{30}(p)] & \Im_m[F_{29}(p)] \end{vmatrix}}{\Delta_{gv}} \quad (79)$$

$$K_{iv} = \frac{\begin{vmatrix} \Re_e[F_{28}(p)] & -\Re_e[F_{30}(p)] \\ \Im_m[F_{28}(p)] & -\Im_m[F_{30}(p)] \end{vmatrix}}{\Delta_{gv}} \quad (80)$$

where

$$\Delta_{gv} = \begin{vmatrix} \Re_e[F_{28}(p)] & \Re_e[F_{29}(p)] \\ \Im_m[F_{28}(p)] & \Im_m[F_{29}(p)] \end{vmatrix} \quad (81)$$

As before, substituting $p = (-\sigma + j\omega)$ in (79)–(81) and varying ω from $-\infty$ to $+\infty$ for fixed σ, the D-partition boundary has been plotted as shown in Fig. 9 (a) and the probable zone of stability in the sense of shading has been obtained in the parametric-plane. The stability of the shaded zone has further been confirmed by the frequency scanning technique for the points outside and inside the shaded zone. For frequency-scanning, the loci of the characteristic vector $D_{GV}(p) = K_{pv}F_{28}(p) + K_{iv}F_{29}(p) + F_{30}(p)$ for the points ($\sigma = 0.0, K_{pv} = 1.0, K_{iv} = 1500$) and ($\sigma = 0.0, K_{pv} = 1.5, K_{iv} = 500$) located outside and inside the shaded zone, respectively are shown in Fig. 9 (b)–(c). It can be confirmed

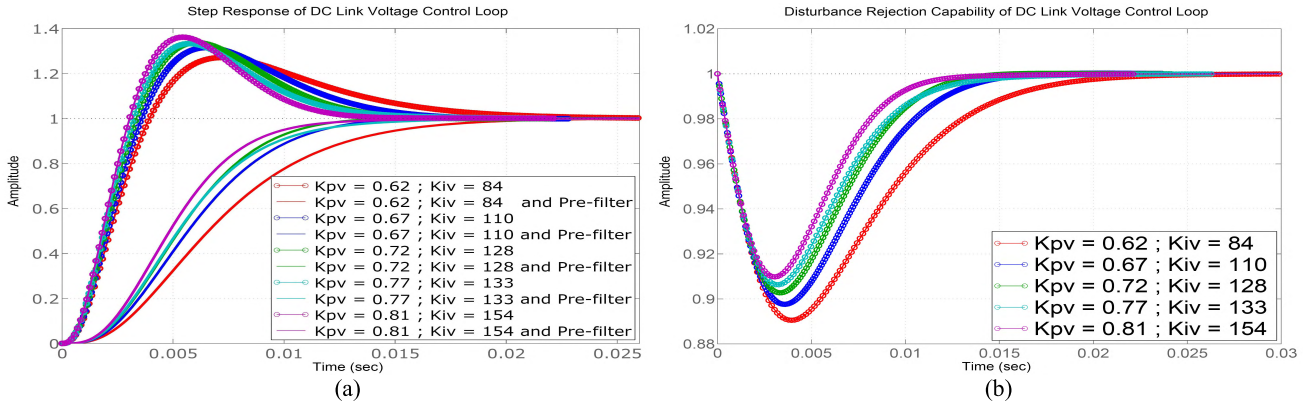

FIGURE 10. (a) Step responses and (b) disturbance rejection capability of the dc-link voltage control loop for different sets of K_{pv} an K_{iv} d values chosen from common portion of the most stable zones in Fig. 9.

TABLE 3. Performance of the dc-link voltage control loop corresponding to different sets of K_{pv} and K_{iv} value.

K_{pv}	K_{iv}	T_{iv}	Step Response				Disturbance Rejection Capability	
			Without Pre-filter		With Pre-filter			
			Overshoot (%)	Settling Time (ms)	Overshoot (%)	Settling Time (ms)	Undershoot (%)	Settling Time (ms)
0.62	84	0.0074	27.1	19.3	---	18.2	10.90	20.4
0.67	110	0.0061	31.5	15.7	0.214	13.3	10.20	15.0
0.72	128	0.0056	33.7	14.1	0.117	12.0	9.73	13.3
0.77	133	0.0058	35.0	14.0	---	14.0	9.37	15.1
0.81	154	0.0053	36.1	12.3	---	11.9	9.02	12.4

that the shaded zone is stable in the parametric-plane and any point within it can be considered as a stable point.

To ensure the maximum relative system stability, σ has gradually been increased and the D-partition boundaries have been plotted as depicted in Fig. 9(a) in order to identify the most stable zone.

Here, the innermost zone shaded with the red color in Fig. 9(a) is the most stable zone with high-degree of relative system stability. The D-partition boundary has also been plotted by substituting $p = \left(-\xi\omega_n + j\omega_n\sqrt{1-\xi^2}\right)$ in (79)–(81) for the fixed value of damping ratio ($\xi > 0$) and probable zone of stability in the sense of shading is obtained as shown in Fig. 9(d). The stability of the shaded zone can further be confirmed by the frequency scanning technique for the points outside and inside the shaded zone. For frequency scanning, the loci of the characteristic vector for the points ($\xi = 0.1, K_{pv} = 0.5, K_{iv} = 600$) and ($\xi = 0.1, K_{pv} = 2.5, K_{iv} = 400$) located outside and inside the shaded zone, respectively are shown in Fig. 9 (e)–(f) and it can be confirmed that the shaded zone is stable in the parametric plane.

To ensure high damping ratio, ξ has gradually been increased and the D-partition boundaries have been plotted as depicted in Fig. 9(d) so as to identify the most stable zone. Here, the innermost zone shaded with the red color in Fig. 9(d) is the most stable zone with specified damping ratio. The final selection of the dc-link voltage PI controller parameters has been made by comparing the step response curves as well as investigating the disturbance rejection capability of the dc-link voltage control loop as shown in Fig. 10 for different sets of K_{pv} and K_{iv} values chosen from the common portion of the most stable zones in Fig. 9 identified earlier to ensure the desired relative system stability and damping ratio respectively. Large peak overshoots in the step responses of the dc-link voltage control loop can be observed. So, a first order pre-filter $G_{FGV}(p)$ can also be employed on the reference signal which decreases the peak overshoot [8] and enhances the performance of the dc-link voltage PI controller.

$$G_{FGV}(p) = \frac{K_{iv}}{K_{iv} + pK_{pv}} \tag{82}$$

Thus, the closed-loop transfer function $G_{CGV}(p)$ reduces to

$$G_{CFGV}(p) = G_{FGV}(p) \cdot G_{CGV}(p) \tag{83}$$

The performance of the dc-link voltage control loop corresponding to different sets of K_{pv} and K_{iv} values have been summarized in Table-3. On comparison, it has been found that the step response curve (with pre-filter on the reference signal) corresponding to ($K_{pv} = 0.81$ and $K_{iv} = 154$) settles very fast with minimum percentage peak overshoot. Further, the disturbance rejection capability of the dc-link voltage control loop is also the best corresponding to ($K_{pv} = 0.81$ and $K_{iv} = 154$). Hence, the selected transfer function of the dc-link voltage PI controller is given by

$$G_{cv}(p) = 0.81\left(\frac{1 + 0.0053p}{0.0053p}\right) \tag{84}$$

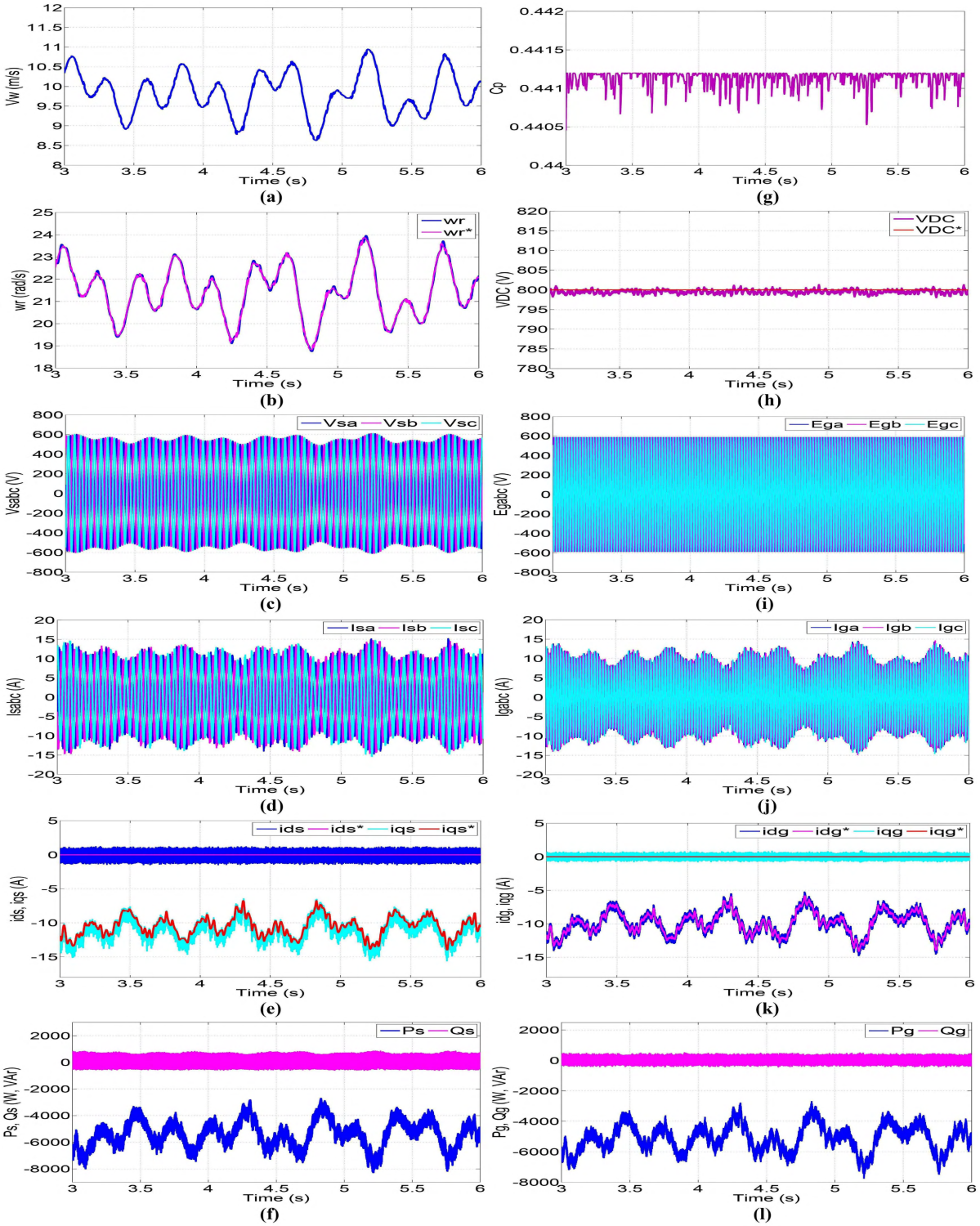

FIGURE 11. Demonstrating the effectiveness of the designed parameters of PI controllers for a grid-interfaced PMSG-based wind energy system under fluctuating wind condition (a) wind speed (b) rotor / turbine-shaft speed (c) three-phase stator voltages (d) three-phase stator currents (e) d-and q-axes stator current components (f) generator active and reactive powers (g) power coefficient (h) dc-link voltage (i) three-phase grid voltages (j) three-phase grid currents (k) d-and q-axes grid current components (l) active and reactive powers transferred to the power grid.

In a recent publication [4], Tripathi *et al.* investigated that the tuning of involved PI controller parameters (in the field-oriented and voltage-oriented control structures of a grid-interfaced PMSG-based WES) using 'symmetrical optimum (SO) criterion with a = 2.4142' offers optimum dynamic responses. It is also interesting to notice the fact

TABLE 4. Comparison of the design of involved PI controller parameters.

Control Loop	Parameters	Involved PI controller parameters designed using	
		D-partition technique	Symmetric optimum (SO) criterion with $a = 2.4142$ [4]
PMSG rotor speed control loop	K_{ps}	5.98	5.90
	T_{is}	0.0029	0.0029
Grid-current control loop	K_{pc}	69.00	70.69
	T_{ic}	0.00043	0.00044
Dc-link voltage control loop	K_{pv}	0.81	0.69
	T_{iv}	0.0053	0.0055

from Table-4 that the PI controller parameters designed in [4] using SO criterion with a = 2.4142 are comparable with the same designed using the D-partition technique. Unlike the SO criterion (which does require the higher-order plant model to be approximated with some benchmark transfer function [4]), the D-partition technique serves as an effective means for the designing and coordination of the PI controller parameters in the parametric plane ensuring high-degree of relative system stability and good damping ratio irrespective of the order of the control system.

IV. MATLAB-BASED SIMULATION, RESULTS AND DISCUSSIONS

To verify the effectiveness of the designed parameters of PI controllers, the grid-interfaced PMSG-based WES using 2-level VSCs has been designed and modelled using MATLAB/Simulink and SimPowerSystems toolbox. The simulations have been performed and the performance of the WES has been observed for fluctuating wind speeds. The simulation results have been shown in Fig. 11. Corresponding to a fluctuating wind speed profile, the consequent variation in the rotor speed, stator voltages, stator currents and average active power generation can easily be observed from Fig.11. On the other hand, the average reactive power generation can be observed zero. The actual d-and q-axes stator current components correctly track their reference values. Irrespective of the fluctuations in the wind speed, the power coefficient maintained itself at about optimum value of 0.4412. Moreover, the dc-link voltage and the grid voltages also remain maintained at their nominal value of 800 V and 415V (r.m.s.), respectively. The variation in the wind speed has an effect directly on the amount of the grid currents and hence, also on the average active power transferred to the grid by the LSC. Upon observing the simulation results in Fig.11, it is worth remarkable that the average active power transferred to the grid has been observed very close that of the average active power generation by the PMSG while, the average reactive power transferred to / absorbed from the power grid can be observed zero throughout. This demonstrates good dynamics and effective design of the parameters of PI controllers for proposed WES.

V. CONCLUSIONS

The D-partition technique was used for the design of the parameters of PI controllers employed in the field-oriented and voltage-oriented control structures of a grid-interfaced variable-speed PMSG-based WES via identifying the most stable zones in the parametric-plane. The final selection of the parameters of PI controllers were carried out by comparing the performance of each control-loop corresponding to different sets of PI controller parameter values chosen from the identified common portion of the most stable zones in order to ensure the high-degree of relative system stability and good damping ratio. The parameters of the PI controllers designed using the D-partition technique were found comparable with the same designed in [4] using the SO design criterion with $a = 2.4142$. The designed parameters of the PI controllers were applied in a simulation model build using MATLAB/Simulink and SimPowerSystems toolbox. The simulation results were presented for fluctuating wind speed condition. The performance of the proposed WES was found satisfactory which verifies the effective design of the parameters of PI controllers in different control-loops. This way, the D-partition technique has established itself as an effective means for the designing and coordination of the PI controller parameters in the parametric-plane irrespective of the order of the control system.

APPENDIX

A. SPECIFICATIONS OF THE PMSG-BASED WES [4]

$P_m = 7.68$ kW; $C_{p\max} = 0.4412$; $\lambda_{opt} = 5.66$; $R = 2.6$ m; $\rho = 1.229$ kg/m^2; $R_s = 1.4\Omega$; $L_d \approx L_q = 5.8$ mH; $\lambda_m = 2.6$ Wb; $P = 12$; $J = 1$ kg-m^2; $R_g = 1.85\Omega$; $L_g = 12.8$ mH; $C = 1000$ μF; $V_{DC}^* = 800$ V; $E_g = 415$ V(r.m.s.); $f = 50$ Hz.

REFERENCES

[1] S. Sharma and B. Singh, "Control of permanent magnet synchronous generator-based stand-alone wind energy conversion system," *IET Power Electron.*, vol. 5, no. 8, pp. 1519–1526, 2012.

[2] S. M. Tripathi, A. N. Tiwari, and D. Singh, "Grid-integrated permanent magnet synchronous generator based wind energy conversion systems: A technology review," *Renew. Sustain. Energy Rev.*, vol. 51, pp. 1288–1305, Nov. 2015.

[3] M. Singh and A. Chandra, "Application of adaptive network-based fuzzy inference system for sensorless control of PMSG-based wind turbine with nonlinear-load-compensation capabilities," *IEEE Trans. Power Electron.*, vol. 26, no. 1, pp. 165–175, Jan. 2011.

[4] S. M. Tripathi, A. N. Tiwari, and D. Singh, "Optimum design of proportional-integral controllers in grid-integrated PMSG-based wind energy conversion system," *Int. Trans. Elect. Energy Syst.*, vol. 26, no. 5, pp. 1006–1031, May 2016.

[5] K. J. Astrom and T. Hagglund, *PID Controllers: Theory, Design, and Tuning*, 2nd ed. Research Triangle Park, NC, USA: Instrument Society America, 1995.

[6] B. Zigmund, A. Terlizzi, X. T. Garcia, R. Pavlanin, and L. Salvatore, "Experimental evaluation of PI tuning techniques for field oriented control of permanent magnet synchronous motors," *Adv. Elect. Electr. Eng.*, vol. 5, no. 3, pp. 114–119, 2006.

[7] K. G. Papadopoulos and N. I. Margaris, "Extending the symmetrical optimum criterion to the design of PID type-*p* control loops," *J. Process Control*, vol. 22, no. 1, pp. 11–25, 2012.

[8] C. Bajracharya, M. Molinas, J. A. Suul, and T. M. Undeland, "Understanding of tuning techniques of converter controllers for VSC-HVDC," in *Proc. Nordic Workshop Power Ind. Electron.*, Jun. 2008, p. 8.

[9] M. A. Johnson and M. H. Moradi, Eds., *PID Control New Identification and Design Methods*. London, U.K.: Springer-Verlag, 2005.

[10] A. O'Dwyer, *Handbook of PI and PID Controller Tuning Rules*, 2nd ed. London, U.K.: Imperial College Press, 2006.

[11] J. Nanda, "Analysis of steady state stability of a two machine system by the D-decomposition technique," in *Proc. IEEE Winter Power Meeting*, Jan./Feb. 1971, pp. 1848–1855.

[12] A. K. Pandey and S. M. Tripathi, "Determination of regulator parameters and transient analysis of modified self-commutating CSI-fed IM drive," *J. Elect. Eng. Technol.*, vol. 6, no. 1, pp. 48–58, 2011.

[13] J. Nanda, "Optimization of voltage regulator gains by the D-decomposition technique for best steady state stability," in *Proc. IEEE Winter Power Meeting*, vol. 5. Jan./Feb. 1971, pp. 2488–2494.

[14] M. A. Aizerman, *Theory of Automatic Control*. New York, NY, USA: Pergamon Press, 1963, ch. 3.

[15] Y. I. Neimark, "Search for the parameter values that make automatic control system stable," *Autom. Telem*, vol. 9, no. 3, pp. 190–203, 1948.

[16] D. D. Siljak, "Analysis and synthesis of feedback control systems in the parameter plane i-linear continuous systems," *IEEE Trans. Appl. Ind.*, vol. 83, no. 75, pp. 449–458, Nov. 1964.

[17] D. Siljak, "Generalization of the parameter plane method," *IEEE Trans. Autom. Control*, vol. 11, no. 1, pp. 63–70, Jan. 1966.

[18] D. Siljak, *Nonlinear Systems: The Parameter Analysis and Design*. New York, NY, USA: Wiley, 1969.

[19] M. S. R. Murty and M. V. Hariharan, "Analysis and improvement of the stability of a hydro-turbine generating unit with long penstock," *IEEE Trans. Power App. Syst.*, vol. PAS-103, no. 2, pp. 360–367, Feb. 1984.

[20] A. T. Shenton and Z. Shafiei, "Relative stability for control systems with adjustable parameters," *J. Guid., Control Dyn.*, vol. 17, no. 2, pp. 304–310, Mar./Apr. 1994.

[21] M. A. Pai and K. Ganesan, "Relative stability of load frequency control system," in *Proc. IEEE Summer Meeting Int. Symp. High Power Test.*, Portland, OR, USA, Jul. 1971, pp. 2734–2741.

[22] J. Spal, "Generalization of the method of D-decomposition," *Kybernetika*, vol. 15, no. 6, pp. 429–445, 1979.

[23] P. Agrawal, A. K. Pandey, and V. K. Verma, "Parameter plane synthesis of a current source inverter fed," *IE (I) J.-EL*, vol. 81, pp. 211–219, Mar. 2001.

[24] P. Agarwal and V. K. Verma, "Parameter coordination of microcomputer controlled CSI fed induction motor drive," *IE (I) J.-EL*, vol. 88, pp. 25–34, Dec. 2007.

[25] A. Ruszewski and T. Nartowicz, "Stabilization of inertial plant with time delay using fractional order controller," *Acta Mech. et Autom.*, vol. 5, no. 2, pp. 117–121, 2011.

[26] K. M. Yanev and S. Masupe, "Robust design and efficiency in case of parameters uncertainties, disturbances and noise," *Int. Rev. Autom. Control*, vol. 5, no. 6, pp. 860–867, Nov. 2012.

[27] L. Dubonjić, N. Nedić, V. Filipović, and D. Prsić, "Design of PI controllers for hydraulic control systems," *Math. Problems Eng.*, vol. 2013, Feb. 2013, Art. no. 451312.

[28] Y. Yang and H. Zhu, "Robust stability regions of PID parameters for uncertainty systems with time delay using D-partition technique," *J. Comput. Inf. Syst.*, vol. 9, no. 20, pp. 8227–8234, 2013.

[29] M. Singh, V. Khadkikar, and A. Chandra, "Grid synchronization with harmonics and reactive power compensation capability of a permanent magnet synchronous generator-based variable speed wind energy conversion system," *IET Power Electron.*, vol. 4, no. 1, pp. 122–130, 2011.

[30] A. N. Tiwari, P. Agarwal, and S. P. Srivastava, "Performance investigation of modified hysteresis current controller with the permanent magnet synchronous motor drive," *IET Electr. Power Appl.*, vol. 4, no. 2, pp. 101–108, 2010.

[31] G. C. Hsich and J. Hung, "Phase-locked loop techniques-A survey," *IEEE Trans. Ind. Electron.*, vol. 43, no. 12, pp. 609–615, Dec. 1996.

[32] E. N. Gryazina, B. T. Polyak, and A. A. Tremba, "D-decomposition technique State-of-the-art," *Autom. Remote Control*, vol. 69, no. 12, pp. 1991–2026, 2008.

SAURABH MANI TRIPATHI was born in Amethi, India, in 1984. He received the B.Tech. degree in electrical and electronics engineering from the G. L. A. Institute of Technology and Management, Mathura, India, in 2006, the M.Tech. degree in power electronics and drives from the M. M. M. Engineering College (now M. M. M. University of Technology), Gorakhpur, India, in 2009, and the Ph.D. degree in electrical engineering from Dr. A. P. J. Abdul Kalam Technical University, Lucknow, India, in 2016. He is currently an Assistant Professor of Electrical Engineering at the Kamla Nehru Institute of Technology, Sultanpur, India. He has authored three engineering books, namely *A Course in Modern Control System* (Laxmi Publications, India), *Modern Control Systems: An Introduction* (Jones and Bartlett Learning, USA), and *Analysis of Basic Systems* (Laxmi Publications, India). He has published over 35 research papers in reputed international/national journals and conferences as well. His areas of current interest include renewable energy systems and electric drives.

AMAR NATH TIWARI was born in Amethi, India, in 1965. He received the B.Tech. degree in electrical engineering from the Regional Engineering College, University of Calicut, Kerala, India, in 1988, the M.Tech. degree in electrical engineering from IIT Kanpur, Kanpur, and the Ph.D. degree in electrical engineering from IIT Roorkee, Roorkee, India, in 1996 and 2003, respectively. In 1989, he joined the Department of Electrical Engineering, M. M. M. Engineering College (now M. M. M. University of Technology), Gorakhpur, India, as a Lecturer, where he has been an Associate Professor since 2006. He has contributed over 65 research papers in national/international journals and conferences. His current interests include power electronics, electrical machines and drives, power quality, and renewable energy. He is a Fellow of the Institution of Engineers, India, and the Institution of Electronics and Telecommunication Engineers, India. He is also a Life Member of the Indian Society for Technical Education.

DEEPENDRA SINGH received the B.Tech. degree in electrical engineering from HBTI, Kanpur, India, the M.E. degree in electrical engineering from the University of Roorkee, Roorkee, India, and the Ph.D. degree in electrical engineering from the U. P. Technical University, Lucknow, India, in 1997, 1999, and 2009, respectively. In 2000, he joined the Department of Electrical Engineering, Kamla Nehru Institute of Technology, Sultanpur, India, as a Lecturer, where he is currently a Professor. He has contributed over 50 research papers in national/international journals and conferences as well. His current research interests include distributed generation and power electronics and drives.